

Scaling Behavior of Angular Dependent Resistivity in CeCoIn₅: Possible Evidence for d-Wave Density Waves

T. Hu,¹ H. Xiao,¹ T. A. Sayles,² M. B. Maple,² Kazumi Maki,³ B. Dóra,⁴ and C. C. Almasan¹

¹*Department of Physics, Kent State University, Kent, OH 44242, USA*

²*Department of Physics, University of California at San Diego, La Jolla, CA 92093, USA*

³*Department of Physics and Astronomy, University of Southern California, Los Angeles, CA 90089-0484, USA and*

⁴*Department of Physics, Budapest University of Technology and Economics, H-1521 Budapest, Hungary*

(Dated: September 25, 2018)

In-plane angular dependent resistivity ADR was measured in the non-Fermi liquid regime of CeCoIn₅ single crystals at temperatures $T \leq 20$ K and in magnetic fields H up to 14 T. Two scaling behaviors were identified in the low-field region where resistivity shows a linear T dependence, separated by a critical angle θ_c which is determined by the anisotropy of CeCoIn₅; i.e., ADR depends only on the perpendicular (parallel) field component below (above) θ_c . These scaling behaviors and other salient features of ADR are consistent with d-wave density waves.

The recently discovered heavy fermion compound CeCoIn₅¹ has generated a lot of interest, partly due to the many analogies present between this compound and the high transition temperature T_c superconductors. Like the cuprates, CeCoIn₅ has a layered crystal structure², a quasi-two-dimensional electronic spectrum^{1,3}, and a superconducting phase appearing at the border of the antiferromagnetic phase⁴. NMR Knight shift^{5,6} and heat conductivity⁷ measurements revealed even parity pairing consistent with d -wave pairing symmetry, while specific heat^{8,9} and electrical transport¹⁰ experiments have shown typical non-Fermi liquid behavior and have evoked the possibility of a pseudogap. In fact, infrared spectroscopy studies have revealed the development of a gap in the density of electronic states of CeCoIn₅ below ~ 100 K¹¹. As in the case of cuprates, all these features suggest the existence of quantum critical phenomena¹². However, the Fermi surface topology is much more complex than in cuprates, with multiple sheets, which implies the participation of several bands in the pairing process^{13,14,15}.

In this complex picture, the nature of the normal state in both systems is not trivial. Until recently, the nature of the pseudogap (or the non-Fermi liquid) phase present in CeCoIn₅ has not been addressed. The giant Nernst effect found in this material above T_c ¹⁶, however, reopened the problem of the origin of the pseudogap state, not only in this compound, but also in the cuprates. It has recently been shown that the giant Nernst effect in CeCoIn₅ is consistent with unconventional density waves UDW or d-wave density waves d-DW¹⁷. We recall that in underdoped cuprates, the pseudogap phase has been attributed to the existence of phase fluctuations of the superconducting order parameter^{18,19,20,21,22} as well as d-DW^{23,24,25}. In particular, the giant Nernst effect observed in La_{2-x}Sr_xCuO₄, YBa₂Cu₃O_{7- δ} , and Bi₂Sr₂CaCu₂O_{8+ δ} has recently been interpreted satisfactorily in terms of d-DW²⁶.

Here, we present new information concerning the nature of the pseudogap of CeCoIn₅ through angular dependent resistivity ADR. Two different scaling behaviors are revealed in this compound in the non-Fermi liquid

regime for applied magnetic fields less than 5 T. Specifically, for angles below (above) a certain critical angle θ_c , the field component perpendicular (parallel) to the ab -planes determines the angular-dependent dissipation. The critical angle θ_c is determined by the anisotropy of the material. These results and the other salient features of ADR measured in high applied magnetic fields are consistent with d-wave density waves with Landau quantization of the quasiparticle spectrum. Our findings bring further understanding of the underlying physics in the non-Fermi liquid regime of this exotic compound and could also advance the understanding of the pseudogap state of the cuprates.

High quality single crystals of CeCoIn₅ were grown using the flux method. Typical sizes of the crystals are $0.5 \times 0.5 \times 0.1$ mm³ with the c -axis oriented along the smallest dimension. We determined the out-of-plane ρ_c and in-plane ρ_{ab} resistivities using the electrical contact configuration of the flux transformer geometry, as described in Ref.²⁷. The angular dependent resistivity $\rho_{ab}(\theta)$ was measured by rotating the single crystal from $H||c$ -axis to $H||I||a$ -axis, with θ the angle between H and the c -axis. Here we report only in-plane resistivity results.

The angular dependent in-plane resistivity of CeCoIn₅ single crystals was measured in the non-Fermi liquid regime, for $T \leq 20$ K and in magnetic fields H up to 14 T. Figure 1 is a typical contour plot of resistivity obtained from ρ vs θ data measured at different fixed applied magnetic field values and at a temperature of 6 K. A similar topologic contour is obtained over the whole T range investigated. The squares, circles, and triangles correspond to $n = 0.45$, 1, and $2/3$, respectively, which consistent with previously report¹², where n is the exponent of the power-law T dependence of the resistivity; i.e., $\rho(T) = \rho_0 + AT^n$. Note that the contour plot can be divided into three different regions based on the shape of the topologic plots and the values of n . Region I is the rectangular part, for which $n = 1$. This region is the so-called low-field region ($H < 5$ T) for reasons given later on. Region II is the elliptical part, for which $n = 0.45$ and which corresponds to the region around the maximum value of the $\rho(H)$ curves for different angles.

Region III is a large area with $n = 2/3$, which is outside of regions I and II at even higher fields. Region I is more interesting since it represents the typical non-Fermi liquid behavior (for this region $n = 1$) and displays the two scaling behaviors. Therefore, we will discuss the anomalous magnetoresistivity behavior in this region in more detail.

The bottom Inset to Fig. 2(a) shows $\rho(\theta)$ measured in a low magnetic field of 2 T. [Data were measured in region I.] The resistivity decreases as θ increases from 0° , reaches a minimum around 60° , and then displays a peak at 90° . The data of the top Inset to Fig. 2(a) were measured in a high field of 9 T. [Data were measured in region III.] The resistivity increases with increasing angle and displays a shoulder, followed by a peak at 90° .

In the low field region (region I), a spectacular scaling of these data is achieved by plotting the resistivity as a function of the component of the applied magnetic field perpendicular to the ab -planes, i.e., $H_\perp = H \cos \theta$, as shown in the main panel of Fig. 2(a). Note that all the curves measured in $H \leq 5$ T overlap for all θ values between 0° and a critical angle $\theta_c \approx 60^\circ$, marked by the arrows, and deviate from this $H \cos \theta$ scaling at higher angles. This value of the critical angle is independent of temperature and applied magnetic field for the range investigated.

We employed a second protocol to measure resistivity, in which we kept the angle between the magnetic field and the c -axis fixed and scanned the magnetic field. Figure 2(b) shows the resistivity as a function of the field component parallel to the a -axis ($H_\parallel = H \sin \theta$), measured at 6 K for different orientations of H . Note that all the resistivity curves scale this time with $H \sin \theta$ for $\theta > \theta_c \simeq 60^\circ$. Therefore, the resistivity data follow two scaling laws:

$$\rho(H, \theta) = \begin{cases} f_1(H \cos \theta) & \text{for } \theta \leq \theta_c \approx 60^\circ \\ f_2(H \sin \theta) & \text{for } \theta \geq \theta_c \approx 60^\circ. \end{cases} \quad (1)$$

Figure 1 also clearly shows the presence of the two scaling laws in region I as evidenced by the rectangular region of the ρ contours. The presence of these two scaling behaviors indicates that below (above) the critical angle, the field component perpendicular (parallel) to the ab -planes determines the in-plane dissipation. A similar analysis of the angular dependent resistivity data measured in high magnetic fields (region III) has shown that the data are still dominated by the perpendicular (parallel) field component below (above) the critical angle, although the two scaling laws are no longer present.

Next we try to understand the above shape of $\rho(\theta)$ measured in both low and high fields and the relationship between the two scaling behaviors. We plot in the Inset to Fig. 3 the resistivity measured at 6 K in scanning H up to 14 T at the two fixed angles ($\theta = 0^\circ$ and $\theta = 90^\circ$) corresponding to the two field orientations (perpendicular and parallel, respectively, to the ab -planes) which seem to determine the physics below and above θ_c , respectively. For the first field orientation ($H \perp ab$

planes), $\rho(H_\perp)$ increases with increasing H_\perp , reaches a maximum around 5 T, and decreases with further increasing H_\perp . We define the low (high) field region as the field region for which $H_\perp < 5$ T ($H_\perp > 5$ T), based on this behavior of $\rho(H_\perp)$. This $\rho(H_\perp)$ dependence gives a qualitative explanation of the $\rho(\theta)$ dependence [shown in the two Insets to Fig. 2(a)] for $\theta < \theta_c$, i.e., at angles at which the dissipation is dominated by the perpendicular field component $H_\perp = H \cos \theta$. Namely, at constant H , the resistivity should decrease (increase) with increasing θ , i.e., decreasing H_\perp , for fields lower (higher) than 5 T as, indeed, shown by the bottom (top) Inset to Fig. 2(a) for $\theta < \theta_c$.

For the second field orientation ($H \parallel a$ -axis), the $\rho(H_\parallel)$ data of the Inset to Fig. 3 show an initial increase with increasing H_\parallel followed by a tendency to saturation for H_\parallel approaching 14 T. This monotonic $\rho(H_\parallel)$ dependence explains qualitatively the increase in $\rho(\theta)$ [shown in the two Insets to Fig. 2(a)] for $\theta > \theta_c$, i.e., at angles at which the dissipation is dominated by the parallel field component $H_\parallel = H \sin \theta$, in both low and high field regimes. In summary, the $\rho(H_\perp)$ and $\rho(H_\parallel)$ dependences of the Inset to Fig. 3 explain the non-monotonic $\rho(\theta)$ dependence at low fields and the monotonic $\rho(\theta)$ dependence at high fields, as shown by bottom and top Inset, respectively, to Fig. 2(a).

Figure 3 shows that the two resistivity curves of its Inset, $\rho(H_\perp)$ and $\rho(H_\parallel)$, scale for $H < 4$ T if $\rho(H_\parallel)$ is replaced by $\rho(\gamma^{-1} H_\parallel)$, with $\gamma = 1.7$. The physical meaning of γ is the anisotropy of the material. The scaling of Fig. 3 implies that the same physics is responsible for the two scaling behaviors displayed by Figs. 1 and 2 for $H < 4$ T, i.e., $f_1(H \cos \theta)$ and $f_2(H \sin \theta)$, respectively.

The scaling relationship of Fig. 3 also allows one to determine the critical angle θ_c below (above) which the resistivity data scale when plotted vs the perpendicular (parallel) component of the applied magnetic field (Figs. 2(a) and 2(b)). Recall that Eq. (1) gives: $f_1(H \cos \theta_c) = f_2(H \sin \theta_c)$. This latter relationship and the scaling of Fig. 3 [$f_1(H) = f_2(\gamma^{-1} H)$ for $H < 4$ T] give $f_1(H \cos \theta_c) = f_1(\gamma^{-1} H \sin \theta_c)$. Therefore, $\theta_c = \tan^{-1} \gamma = 59.5^\circ$ with $\gamma = 1.7$, as determined above. This value of the critical angle is in excellent agreement with the 60° value obtained experimentally, which proves the consistency of our analysis of the angular and field dependent data. So, the critical angle is given by the anisotropy of the material.

The scaling of the magnetoresistivity curves for $H \parallel c$ -axis (for which the Lorentz force is maximum) and for $H \parallel I \parallel a$ -axis (for which the Lorentz force is zero) shown in Fig. 3 implies that the spin effect, rather than the orbital effect, is responsible for the magnetoresistivity in region I. The fact that in this region the resistivity is also linear in T , indicates that this linear T dependence is as well a result of spin fluctuations. This conclusion that spin fluctuations dominate the charge transport in the non-Fermi liquid regime is consistent with recent In-NQR and Co-NMR experiments²⁸, which have revealed

that the magnetic nature in CeCoIn₅ is characterized by strong antiferromagnetic spin fluctuations in the vicinity of the quantum critical point.

In the following, we show that all the observed features of ADR of CeCoIn₅ in the non-Fermi liquid regime, when a magnetic field is rotated from $H||c$ -axis to $H||I||a$ -axis with θ the angle between H and the c -axis, can be consistently described in terms of d-wave density waves in a magnetic field. The unconventional density wave UDW or d-wave density wave d-DW is a kind of density wave in which the gap function $\Delta(\vec{k})$ vanishes on the line nodes. Therefore, the transition from the normal state to the UDW is a metal to metal transition²⁹. The UDW exhibits two characteristics: angular dependent resistivity and giant Nernst effect. A UDW in the low temperature phase of α -(ET)₂KHg(SCN)₄ and the metallic phase of (TMTSF)₂X with X = PF₆ and ReO₄ has been identified through ADR^{30,31}.

We assume that the electrical conductivity in the non-Fermi liquid regime is given by:

$$\rho(H, \theta)^{-1} = \sum_n \sigma_n (\text{Sech}^2(E_n/2k_B T)), \quad (2)$$

where E_n is the energy of all fermionic excitations (holes and particles). As shown below, this new formula appears to be more appropriate than the one used earlier²⁶. In the absence of a magnetic field, we assume that the quasiparticle energy spectrum is given by:

$$E(\vec{k}) = \sqrt{\xi^2 + \Delta^2(\vec{k})}, \quad (3)$$

where $\xi = v(k_{\parallel} - k_F) - (v'/c) \cos(ck_z)$ and $\Delta(k) = \Delta \sin(2\phi)$; here v and v' are Fermi velocities in the ab -plane and along the c -axis, respectively, k_{\parallel} is the radial wave vector within the ab -plane, Δ is the maximum value of the d-DW energy gap $\Delta(k)$, and $\tan \phi = k_y/k_x$. Here we assume that $\Delta(k)$ has d_{xy} -wave symmetry. In the vicinity of the nodal points, it is convenient to replace $\Delta^2 \sin^2(2\phi)$ by $v_2^2 k_{\perp}^2$, where k_{\perp} is perpendicular to k_{\parallel} within the ab plane and $v_2/v = \Delta/E_F$. Then in a magnetic field which makes an angle θ with the c -axis, the energy spectrum becomes³²:

$$E_{1n}^{\pm} = \pm \sqrt{2env_2 H (v|\cos \theta| + v' \sin \theta)} - \mu \quad (4)$$

$$E_{2n}^{\pm} = \pm \sqrt{2env_2 H (v|\cos \theta| - v' \sin \theta)} - \mu. \quad (5)$$

Here E_{1n}^{\pm} and E_{2n}^{\pm} are the two branches of the Landau levels, $n = 0, 1, 2, \dots$, and μ is the chemical potential. We note that in Ref.²⁶ only E_{1n}^{\pm} is considered. The electrical conductivity is then given by:

$$\rho(H, \theta)^{-1} = \sigma_0 + \sum_{i=+, -} \sigma_1 (\text{Sech}^2(x_{11}^i) + \text{Sech}^2(x_{21}^i)), \quad (6)$$

where $x_{11}^{\pm} = E_{11}^{\pm}/2k_B T$ and $x_{21}^{\pm} = E_{21}^{\pm}/2k_B T$. For simplicity, we take only the $n = 0$ and $n = 1$ Landau levels.

Equation (6) fits very well the $\rho(\theta)$ data over the whole range of the applied magnetic field, both in the low and high field regimes. Representative plots of the resistivity data measured in 4, 8, and 10 T along with the fitting curves are shown in Fig. 4. In these fits we assume that

$$\sigma_n = A_n \left[1 + \left(\frac{H}{H_0} \cos \theta \right)^2 \right], \quad (7)$$

with $n = 0, 1$. The fitting parameters determined by fitting the data measured in different magnetic fields are almost constant, hence field independent, as they should be. Their values are: the anisotropy $\gamma = v/v' \approx 1.9$, $\sqrt{vv_2} \approx 1.3 \times 10^4$ m/s, $\mu = 8.4$ K and $H_0 = 20$ T. This value of the anisotropy γ of 1.9 is very close to the value of 1.7 required to scale the data shown in Fig. 3. With $v = 3.3 \times 10^4$ m/s, obtained by fitting the $H_{c2}(T)$ curve of CeCoIn₅³³ and the above value of $\sqrt{vv_2}$, we get $v_2/v = \Delta(0)/E_F \approx 0.1$. Provided that $E_F = 450$ K, this gives $\Delta(0) \approx 45$ K, a value expected from the weak-coupling theory for d-DW with $T_c = 20$ K.²⁹ This overall consistency between the obtained and expected values of the fitting parameters further attests to the appropriateness of the model used to analyze the experimental data.

Moreover, the d-DW model given by Eq. (6) also gives the scaling observed experimentally at $H < 5$ T. Figure 5 is a plot of the $\rho(\theta)$ data (open symbols), the fitting with Eq. (6) (solid line), and the two scalings (dashed lines) calculated from Eq. (6) in which E_{1n}^{\pm} and E_{2n}^{\pm} , Eq. (4) and (5), respectively, include only the $H \cos \theta$ or $H \sin \theta$ terms, for $\theta < 60^\circ$ and $\theta > 60^\circ$, respectively. Note the excellent agreement between the fitting line and the two scaling lines. Therefore, even though the model proposed here is quite complex, it gives the two experimentally observed scaling laws at low magnetic field values.

In summary, comprehensive angular dependent resistivity ADR measurements in the non-Fermi liquid region of CeCoIn₅ at $T \leq 20$ K have shown the presence of two different scaling behaviors in the low-field region (region I) which involve the H and θ dependence and are due to spin fluctuations. The two scaling regions are separated by a critical angle θ_c , which is given by the intrinsic anisotropy. In the scaling region, the resistivity is linear in T . At higher fields, the ADR data are governed by the same physics, even though the two scalings fail. A possible explanation for this anomalous ADR in terms of d-wave density waves with Landau quantization of the quasiparticle spectrum was presented. This approach describes very well the salient features of ADR data: (i) the distinctive angular dependences observed in the low ($d\rho/dH_{\perp} > 0$) and high ($d\rho/dH_{\perp} < 0$) field regimes follow naturally from Eq. (7); (ii) the low field scaling behaviors follow from the quasiparticle spectrum given by Eqs. (4) and (5). In addition, the quasi two dimensional aspect of d-wave density waves is explored here for the first time.

Acknowledgments

This research was supported by the National Science Foundation under Grant No. DMR-0406471 at KSU and

the U. S. Department of Energy under Grant No. DE-FG02-04ER46105 at UCSD. The authors acknowledge useful discussions with Dr. V. Sandu.

-
- ¹ C. Petrovic, P. G. Pagliuso, M. F. Hundley, R. Movshovich, J. L. Sarrao, J. D. Thompson, Z. Fisk, and P. Monthoux, *J. Phys. Condens. Matter* **13**, 337 (2001).
 - ² A. Bianchi, R. Movshovich, I. Vekhter, P. G. Pagliuso, and J. L. Sarrao, *Phys. Rev. Lett.* **91**, 257001 (2003).
 - ³ D. Hall, E. C. Palm, T. P. Murphy, S. W. Tozer, Z. Fisk, U. Alver, R. G. Goodrich, J. L. Sarrao, P. G. Pagliuso, and T. Ebihara, *Phys. Rev. B* **64**, 212508 (2001).
 - ⁴ H. Hegger, C. Petrovic, E. G. Moshopoulou, M. F. Hundley, J. L. Sarrao, Z. Fisk, and J. D. Thompson, *Phys. Rev. Lett.* **84**, 4986 (2000).
 - ⁵ Y. Kohori, Y. Yamato, Y. Iwamoto, T. Kohara, E. D. Bauer, M. B. Maple, and J. L. Sarrao, *Phys. Rev. B* **64**, 134526 (2001).
 - ⁶ N. J. Curro, B. Simovic, P. C. Hammel, P. G. Pagliuso, J. L. Sarrao, J. D. Thompson, and G. B. Martins, *Phys. Rev. B* **64**, 180514(R) (2001).
 - ⁷ K. Izawa, H. Yamaguchi, Y. Matsuda, H. Shishido, R. Settai, and Y. Onuki, *Phys. Rev. Lett.* **87**, 057002 (2001).
 - ⁸ C. Petrovic, R. Movshovich, M. Jaime, P. G. Pagliuso, M. F. Hundley, J. L. Sarrao, Z. Fisk, and J. D. Thompson, *Europhys. Lett.* **53**, 354 (2001).
 - ⁹ J. S. Kim, J. Alwood, G. R. Stewart, J. L. Sarrao, and J. D. Thompson, *Phys. Rev. B* **64**, 134524 (2001).
 - ¹⁰ V. A. Sidorov, M. Nicklas, P. G. Pagliuso, J. L. Sarrao, Y. Bang, A. V. Balatsky, and J. D. Thompson, *Phys. Rev. Lett.* **89**, 157004 (2002).
 - ¹¹ E. J. Singley, D. N. Basov, E. D. Bauer, and M. B. Maple, *Phys. Rev. B* **65**, 161101(R) (2002).
 - ¹² J. Paglione, M. A. Tanatar, D. G. Hawthorn, E. Boaknin, R. W. Hill, F. Ronning, M. Sutherland, L. Taillefer, C. Petrovic, and P. C. Canfield, *Phys. Rev. Lett.* **91**, 246405 (2003).
 - ¹³ D. Hall, E. C. Palm, T. P. Murphy, S. W. Tozer, Z. Fisk, U. Alver, R. G. Goodrich, J. L. Sarrao, P. G. Pagliuso, and T. Ebihara, *Phys. Rev. B* **64**, 212508 (2001).
 - ¹⁴ R. Settai, H. Shishido, S. Ikeda, Y. Murakawa, M. Nakashima, D. Aoki, Y. Haga, H. Harima, and Y. Onuki, *J. Phys. Condens. Matter* **13**, L627 (2001).
 - ¹⁵ J. Costa-Quintana and F. López-Aguilar, *Phys. Rev. B* **67**, 132507 (2003).
 - ¹⁶ R. Bel, K. Behnia, Y. Nakajima, K. Izawa, Y. Matsuda, H. Shishido, R. Settai, and Y. Onuki, *Phys. Rev. Lett.* **92**, 217002 (2004).
 - ¹⁷ B. Dóra, K. Maki, A. Virosztek, and A. Vanyolos, *Phys. Rev. B* **71**, 172502 (2005).
 - ¹⁸ Z. A. Xu, N. P. Ong, Y. Wang, T. Kakeshita, and S. Uchida, *Nature* **406**, 486 (2000).
 - ¹⁹ Y. Wang, Z. A. Xu, T. Kakeshita, S. Uchida, S. Ono, Y. Ando, and N. P. Ong, *Phys. Rev. B* **64**, 224519 (2001).
 - ²⁰ Y. Wang, N. P. Ong, Z. A. Xu, T. Kakeshita, S. Uchida, D. A. Bonn, R. Liang, and W. N. Hardy, *Phys. Rev. Lett.* **88**, 257003 (2002).
 - ²¹ C. Capan, K. Behnia, J. Hinderer, A. G. M. Jansen, W. Lang, C. Marcenat, C. Marin, and J. Flouquet, *Phys. Rev. Lett.* **88**, 056601 (2002).
 - ²² V. Sandu, E. Cimpoeasu, T. Katuwal, S. Li, M. B. Maple, and C. C. Almasan, *Phys. Rev. Lett.* **93**, 177005 (2004).
 - ²³ E. Cappelluti and R. Zeyher, *Phys. Rev. B* **59**, 6475 (1999).
 - ²⁴ L. Benfatto, S. Caprara, and C. D. Castro, *Eur. Phys. J. B* **17**, 95 (2000).
 - ²⁵ S. Chakravarty, R. B. Laughlin, D. K. Morr, and C. Nayak, *Phys. Rev. B* **63**, 094503 (2001).
 - ²⁶ K. Maki, B. Dóra, A. Virosztek, and A. Vanyolos, *Curr. Appl. Phys.* **4**, 693 (2004).
 - ²⁷ C. N. Jiang, A. R. Baldwin, G. A. Levin, T. Stein, C. C. Almasan, D. A. Gajewski, S. H. Han, and M. B. Maple, *Phys. Rev. B* **55**, 3390(R) (1997).
 - ²⁸ Y. Kawasaki, S. Kawasaki, M. Yashima, G. q. Zheng, and Y. Kitaoka, *J. Phys. Soc. Jpn.* **72**, 2308 (2003).
 - ²⁹ B. Dóra, K. Maki, and A. Virosztek, *Mod. Phys. Lett. B* **18**, 327 (2004).
 - ³⁰ K. Maki, B. Dóra, M. Kartsovnik, A. Virosztek, B. Korin-Hamzic, and M. Basletic, *Phys. Rev. Lett.* **90**, 256402 (2003).
 - ³¹ B. Dóra, K. Maki, A. Vanyolos, and A. Virosztek, *Europhys. Lett.* **67**, 1024 (2004).
 - ³² A. A. Nersisyan, G. I. Japaridze, and I. G. Kimeridze, *J. Phys. Condens. Matter* **3**, 3353 (1991).
 - ³³ H. Won, K. Maki, S. Haas, N. Oeschler, F. Weickert, and P. Gegenwart, *Phys. Rev. B* **69**, 180504(R) (2004).

I. FIGURE CAPTION

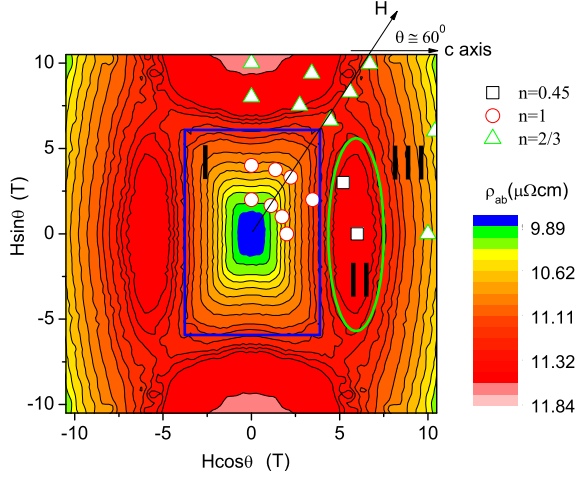


FIG. 1: A contour plot of the in-plane resistivity ρ of CeCoIn_5 in the $H \cos \theta - H \sin \theta$ plane. Three different regions are found in the contour plot, which are distinguished by different values of the exponent n of the power-law T dependence of the resistivity; i.e., $\rho = \rho_0 + AT^n$. The x -axis of this plot is along the c -axis of CeCoIn_5 and θ_c is the angle between the diagonal of the rectangle in region I and the x -axis (c -axis).

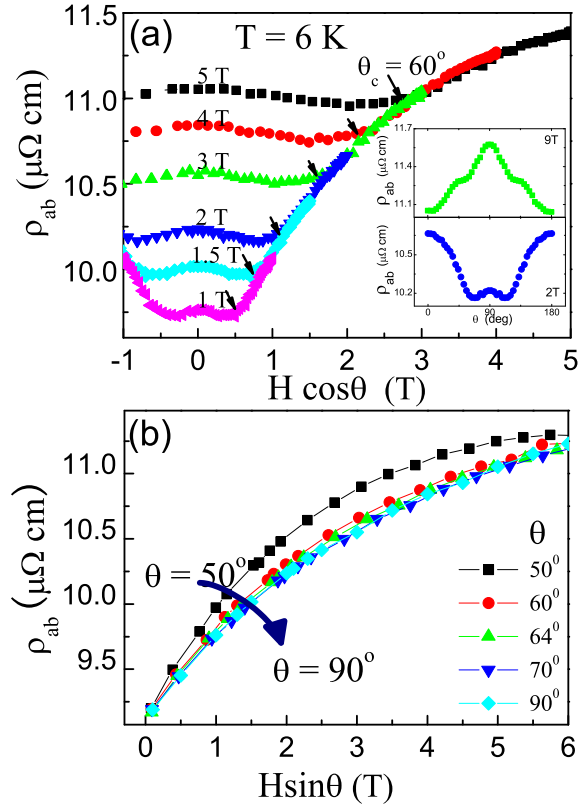


FIG. 2: Figure 2(a) Scaling of resistivity ρ vs the component of the applied magnetic field H perpendicular to the ab -planes, $H \cos \theta$, measured at a temperature T of 6 K and for $1 \text{ T} \leq H \leq 5 \text{ T}$. The arrows mark the points at which the curves start to deviate from each other. Insets: ρ vs the angle θ measured at in an applied magnetic field of 2 T and 9 T. 2(b) Resistivity ρ vs the component of the applied magnetic field H parallel to the ab -planes, $H \sin \theta$, measured at a temperature T of 6 K in scanning H at fixed orientation $50^\circ \leq \theta \leq 90^\circ$. The ρ vs $H \sin \theta$ data scale for $60^\circ \leq \theta \leq 90^\circ$.

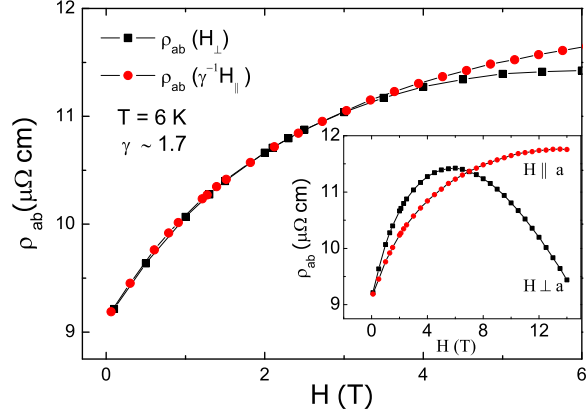


FIG. 3: Figure 3. In region I, scaling of resistivities $\rho(H_{\perp})$ and $\rho(\gamma^{-1}H_{\parallel})$ when plotted vs the component of the magnetic field perpendicular to the ab -planes, H_{\perp} , and parallel to the ab -planes, H_{\parallel} , times the inverse anisotropy γ^{-1} , respectively. Inset: Plots of $\rho(H_{\perp})$ and $\rho(H_{\parallel})$ curves measured in magnetic fields up to 14 T.

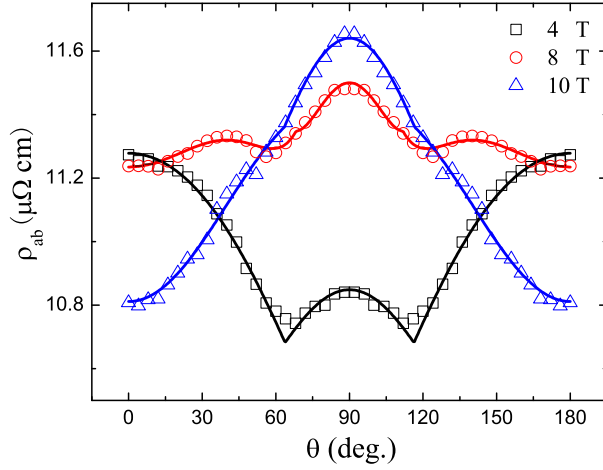


FIG. 4: Figure 4. Angular (θ) dependent resistivity ρ measured at 6 K in a magnetic field of 4 T, 8 T and 10 T. The solid lines are fits of Eq. (6) to the data.

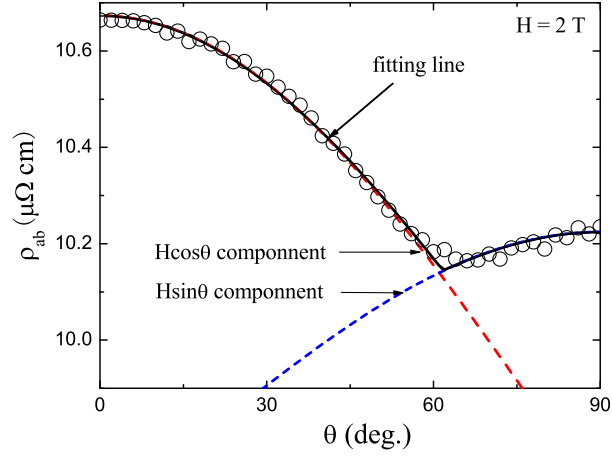


FIG. 5: Figure 5. Angular (θ) dependence of the resistivity ρ measured at 6 K in a magnetic field $H = 2$ T (open symbols). The solid line is the fit of Eq. (6) to the data. The dashed lines are the $H \cos \theta$ and $H \sin \theta$ scalings laws.